A New Dataset Combined Dual Tail Doppler Radars and Compact Raman Lidar Measurements in VORTEX-SE 2018 – A Brief Summary

Guo Lin, Research Scientist
Laboratory for Atmospheric and Space Physics
Department of Atmospheric and Oceanic Sciences
University of Colorado Boulder, CO
3665 Discovery Dr.
Boulder, CO 80303-7819
Contact: Guo.Lin@colorado.edu
ORCID: 0000-0002-4470-8882

and

Zhien Wang, Professor, PI
School of Marine and Atmospheric Sciences, SoMAS,
Stony Brook University,
Stony Brook, NY 11794-5000
Phone: 631-632-8628 (office)
Contact: Zhien.Wang@stonybrook.edu
ORCID: 0000-0003-3871-3834

Grant ID: National Science Foundation (NSF) Grants AGS- 1917693

1. Dataset Overview

The Verification of the Origins of Rotation in Tornadoes Experiment Southeast 2018 (VORTEX-SE 2018 or VSE18) is the third year of the VORTEX-SE research program to characterize environmental factors unique to the southeastern United States. The large purple box in Figure 1 shows the VSE18 domain where the National Oceanic and Atmospheric Administration (NOAA) WP-3D (P-3) Orion aircraft conducted the flights for convective storms (small purple boxes).

The VORTEX-SE program seeks improved understanding relating to how these environmental factors influence the formation, intensity, structure, and path of tornadic storms in this Southeast region. The VORTEX-SE research program was conceived and implemented to provide the greatest possible public benefit, while simultaneously making any future tornado research programs in the Southeast more effective (Rasmussen 2015). For more details, please visit https://www.eol.ucar.edu/field_projects/vortex-se.

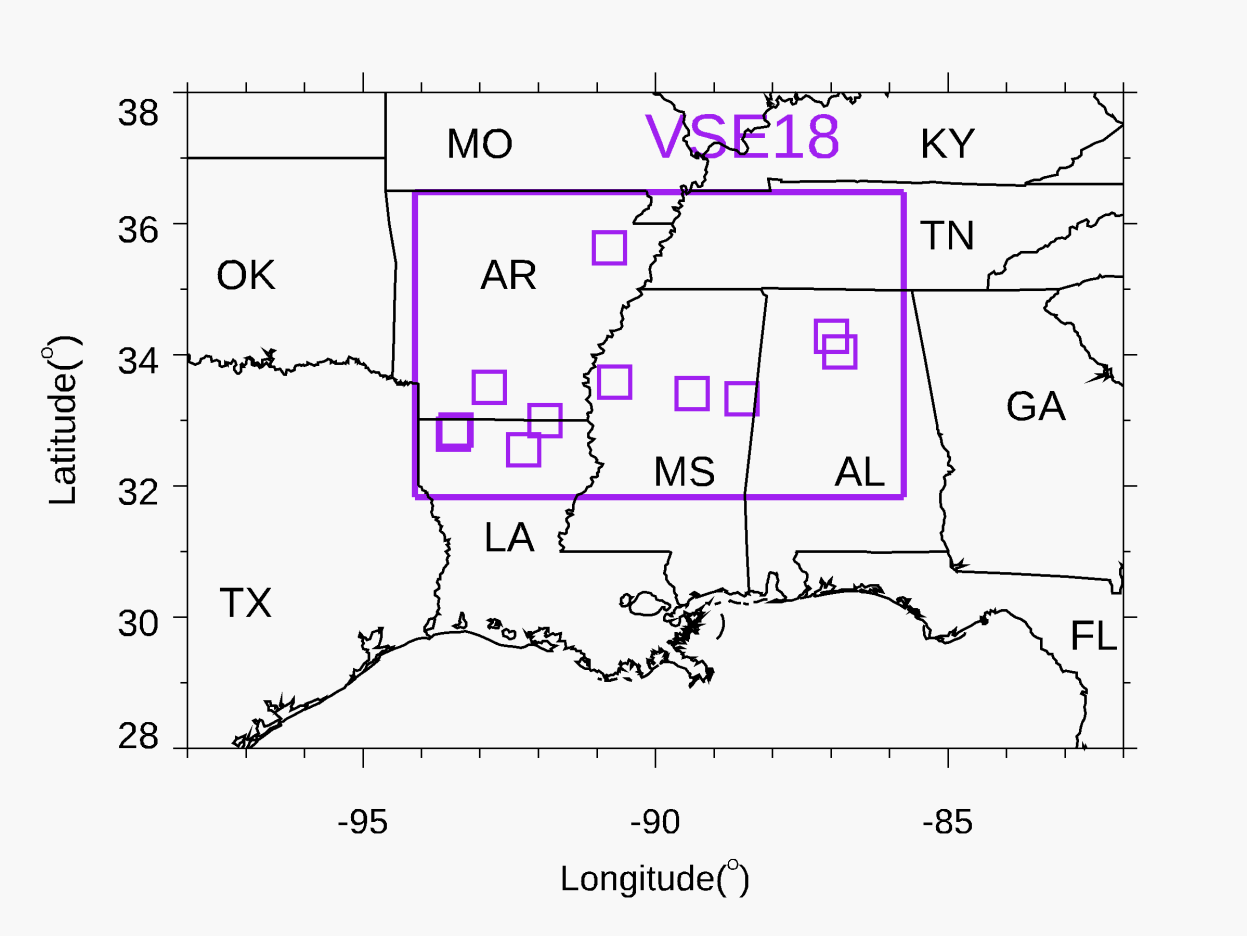

Figure 1. *The VSE18 domain (the large purple box) with NOAA P-3 flight locations (small purple boxes) in the southeastern United States.*

Airborne observations of convective storms over complex terrain are critically useful in documenting storms, their environments, and storm-environment interactions, especially in the Southeast, because traditional ground-based mobile-observation field experimental strategies for sampling storms cannot be easily implemented in the Southeast due to hills, trees, and harder-to-

navigate roads. To supplement the observational needs for understanding deep, moist convective storm inflow processes in the Southeast, one of the National Oceanic and Atmospheric Administration (NOAA) WP-3D (P-3) Orion "Hurricane Hunter" heavy research aircraft (tail number N42RF) was deployed successfully with onboard dual-tail Doppler Radars (TDRs) and the University of Colorado Compact Raman Lidar (CRL) system to sample the inflows and internal structures of fast-moving convective storms in the Southeast during the VSE18 field campaign. The P-3 observations offer a unique dataset with sufficient resolutions to characterize the spatiotemporal moisture variability in convective storm inflows. This document describes this new dataset in characterizing storm dynamics and inflow environments by combining TDRs and CRL systems from March 10 to April 14, 2018. Table 1 summarizes 11 sampled convective storms with information on locations, sampled periods, and legs conducted during the campaign.

Table 1. *Cases of interest with good-quality CRL data during P-3 flight operations, as revealed by numbers of straight flight legs from VSE18. Times are in UTC.*

VORTEX-SE 2018			
Case	Location	Time (UTC)	Straight Legs
1	MS	2216-2250 Mar 10	8
2	MS	2300-2337 Mar 10	7
3	MS	2352-2510 Mar 10/11	12
4	AL	2257-2355 Mar 19	8
5	AL	2357-2421 Mar 19/20	5
6	AR	2216-2324 April 03	10
7	LA	2035-2108 April 13	5
8	LA	2109-2153 April 13	6
9	AR	2158-2234 April 13	8
10	LA	2314-2408 April 13/14	12
11	LA to AR	0014-0134 April 14	14

2. Data Instrument Description

2.1 Tail Doppler Radars

The TDRs deployed on the NOAA P-3 aircraft tail are identical X-band (9.32 GHz) Doppler Radars, which have been used widely to retrieve detailed radar reflectivity and 3D wind in storms by a Dual-Doppler radar wind synthesis method and to characterize hurricanes and continental convective storms. The NOAA P-3 aircraft has two solid-state 360° vertically scanning TDRs with flat-plate antennas whose beams are pointed fore and aft at ±20° relative to a plane perpendicular to the aircraft fuselage (Figure 2a). The simultaneous dual-TDR sampling at 20 deg s^{-1} antenna rotation enables high-resolution dual-Doppler airflow syntheses in interacting areas of the two radars along flight tracks around nearby storms. Each volume of data, representing a vertical cross-section of the storm, was sampled around 3 seconds with a horizontal distance of approximately 360 m (Figure 2b). A typical leg lasts ~5 minutes and is flown at a distance of ~10–20 km from the storm and at a height of ~1 km above ground level. This information can be used to correlate storm features with features in the Doppler analyses.

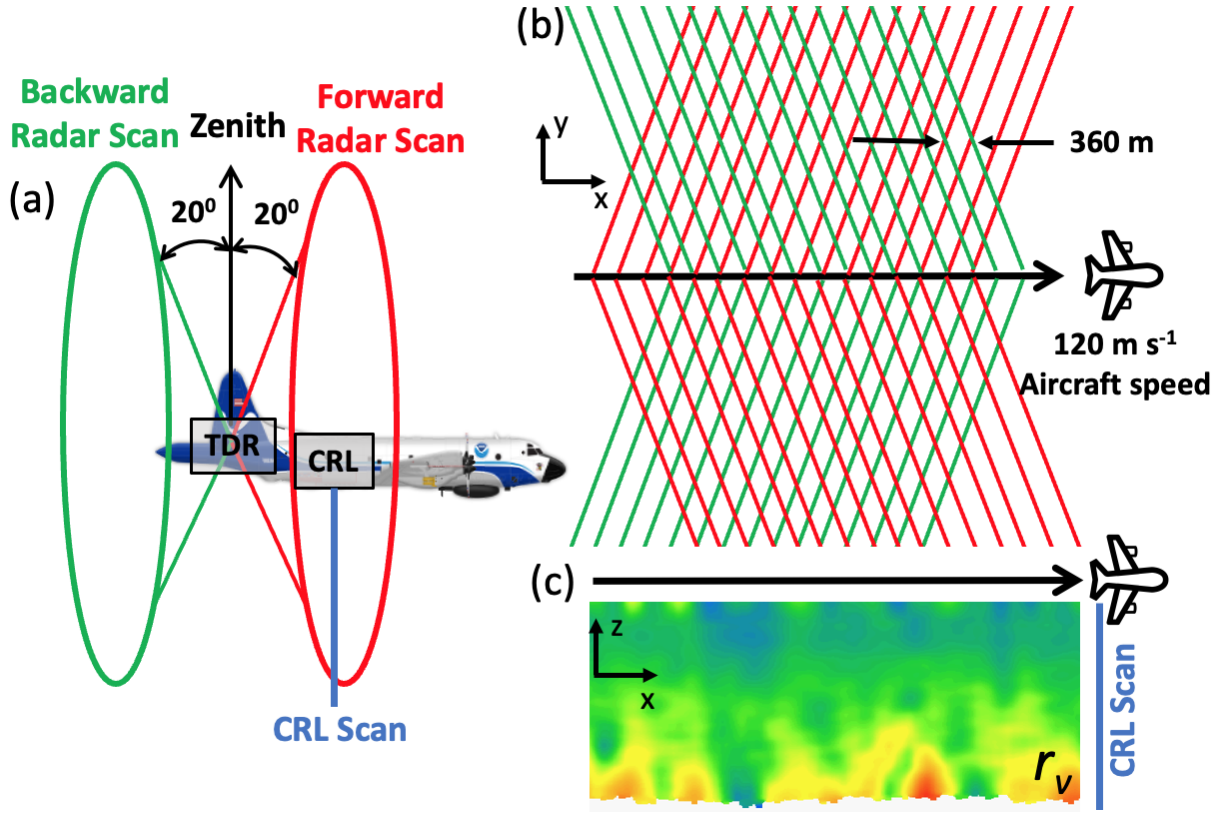

Figure 2. *The schematic figure depicts the scanning strategy for NOAA P-3 dual-TDRs and Compact Raman Lidar (CRL). The red circle represents the volumes scanned by the forward TDR, while the green circle represents the volumes scanned by the backward TDR. The blue vertical line represents the scan by the CRL; The profile of the water vapor mixing ratio (r_v) is shown in (c).*

To create a comprehensive map of 3D wind and radar reflectivity during a flight, dual-Doppler radar synthesis is used to map all data to regular Cartesian grids for forward and backward single TDR radars and then synthesize the gridded forward single-TDR objective data and backward single-TDR objective data for every flight leg in VSE18. The analysis domains of each straight flight segment had a spatial grid separation of 250 m x 250 m x 250 m and a domain size of 401 x 401 x 81 points, covering 100 km in west-east and south-north directions, and 20 km in the vertical direction. This grid spacing corresponds to the longest unresolvable wavelength (i.e., Nyquist wavelength) of 500 m. Numerous studies conducted in the last 20 years have demonstrated that 3-D wind field analyses from airborne radars are sufficient in capturing the wind field of a supercell, particularly previous studies for the mid-levels to the surface where extreme upper-level wind shears made velocity editing difficult. The standard deviation error is approximately 1 m s^{-1} for the horizontal wind, and 2.5 - 5 m s^{-1} for the vertical wind (Bluestein et al. 1997; Ziegler et al. 2001; Jorgensen et al. 2017; Ziegler et al. 2018). The TDR radar capabilities make the NOAA P-3 a unique platform to sample the structure and kinematics of tornadic and non-tornadic convective systems within the VSE18 domain.

2.2 Compact Raman Lidar

The University of Colorado CRL was deployed on the NOAA P-3 during the VSE18 in the Southeast (CRL shown in Figure 3; Lin et al. 2023). The CRL is most sensitive at night (Mueller et al. 2017; Lin et al. 2021) or under low solar background (e.g., with optically thick clouds overhead). Raman scattering, which includes the pure-rotational and vibrational Raman spectra, provides a unique mechanism for remote sensing of multiple atmospheric properties from one system (main parameters in Table 2). The vibrational Raman scattering intensity is fundamentally proportional to the number of molecules involved - a feature widely used to remotely measure atmospheric components (Cooney 1970; Philbrick 1994; Turner and

Whiteman 2006). Because the proportion of nitrogen, relative to other dry air components, is a constant, the ratio of Raman scattering signals from water vapor (407.5 nm) to that from nitrogen (386.7 nm) can be accurately translated to Water Vapor Mixing Ratio (WVMR or r_v with a unit of g kg^{-1}; validated data range of 0-25 g kg^{-1}) after the system constant is calibrated (Whiteman et al. 1992). The intensities of low rotational quantum-number (low-J) transitions of the pure rotational Raman spectrum decrease with increasing temperature, while those of the high quantum-number (high-J) transitions increase. Thus, the atmospheric temperature can be estimated from low-J and high-J rotational Raman channel measurements (Wu et al. 2016). When the sun angle is high, the CRL (whose laser is relatively low-power at 50-mJ) can still provide reliable data over a limited range (up to 1.5 km; the range of mean value could be longer). Past CRL measurements demonstrated that the CRL offers powerful measurements needed to characterize PBL structures from airborne platforms (Bergmaier et al. 2014; Liu et al. 2014; Grasmick et al. 2018; Lin et al. 2019; Lin et al. 2021)

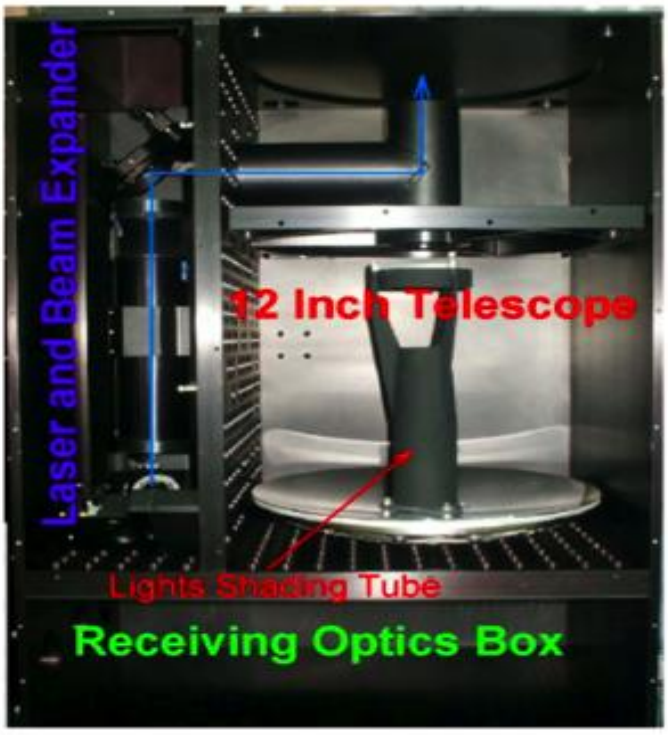

Figure 3*. Photograph of CRL inner structure.*

The CRL performed well on the P-3 during the VSE18, although CRL measurements for the first four VSE18 flights (in March 2018) were degraded by contamination of the optical window by a thin oil film during flight. This compromised water vapor estimates near the surface when the P-3 flew higher than 1.5 km (AGL; hereafter, all heights are Above Ground Level unless explicitly noted), but the typical flight levels were around 1 km during VSE18. The quality control procedure includes masking data points at and around gates with large attenuations of Raman lidar signals by liquid clouds, and r_v estimates larger than 25 g kg^{-1} (impacted by surface). The single shot raw data of CRL provides a 4-m horizontal resolution while the true aircraft speed is around 120 m s^{-1} and up to 0.75-m vertical resolution (Liu et al. 2014). Different horizontal and vertical averaging can be selected during post-data analyses for different measurement targets. The CRL provides accurate retrievals of r_v with a mean difference of 0.2 g kg^{-1} compared to in situ measurements in the lower troposphere at a resolution of ~300 m horizontally and ~100 m vertically (Liu et al. 2014; Wu et al. 2016; Wang 2020). In this study, the horizontal r_v of CRL is smoothed to 1200 m by a 3-second averaging window, and the vertical resolution is 30 m.

Table 2. *Main System parameters of the CRL*

Laser	Nd:YAG laser		
Wavelength	354.7 nm		
Pulse Energy/Width	50 mJ/7ns		
Pulse Repetition Frequency	30 Hz		
Beam Divergence/Expander	1.8 mrad/5X		
Bin Size (Δz)	0.75 m		
Telescope	Cassegrain, 12-inch Diameter		
Filter Central Wavelength	354.7 nm	386.7 nm	407.5 nm
Filter Bandwidth	0.3 nm	0.3 nm	0.3 nm

3. TDR and CRL Data Collection during VSE18

3.1 P-3 Sample Strategy

The P-3 aircraft sampled multiple severe and tornadic storms in the Southeast United States from 10 March to 14 April 2018 during VSE18. An illustrative series of P-3 flight tracks of VSE18 in the near-inflow of a decaying supercell storm in Arkansas on 13 April 2018, including flight-level r_v and 2D r_v vertical profiles below the aircraft, is shown in Figure 4. The top side of the inserted r_v transect in each panel is at nearly ~ 1 km AGL, while the P-3 flight level is about 0.95 km AGL. The radar-indicated storm moved northeastward as the aircraft flew reverse-tracks following the storm motion at a ~10 km storm-setback distance and sampled the near-storm inflow (Fig. 4a-f). The vertical distribution of WVMR, rather than being vertically well-mixed, reveals a complicated profile varying with height in the inflow (Figure 4).

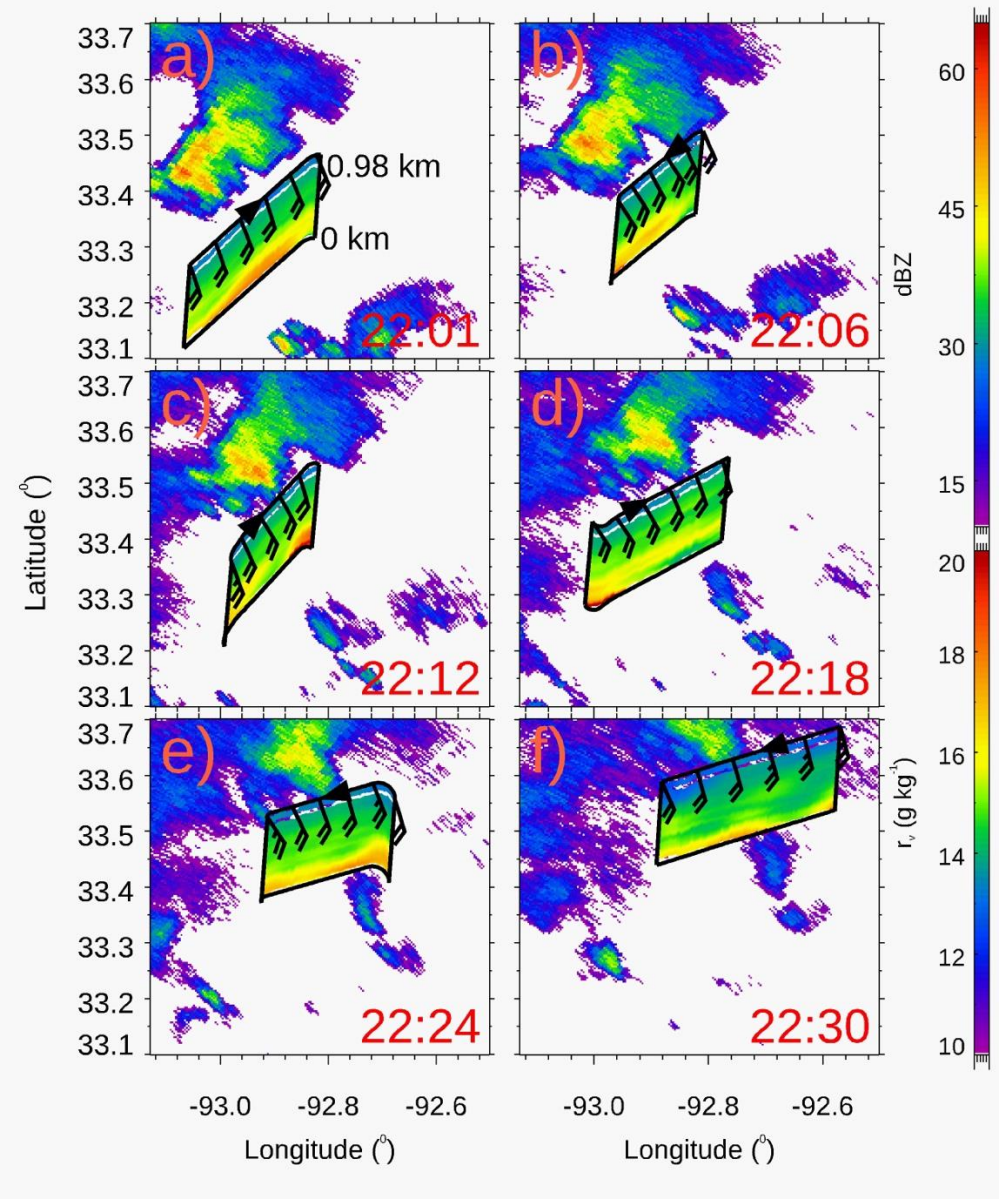

Figure. 4: *Radar base scan (0.5^0) radar reflectivity maps with a vertical r_v profile along the P-3 flight track at (a) 2201, (b) 2206, (c) 2212, (d) 2218, (e) 2224, (f) 2230 UTC on 13 April 2018. The color-coded curves above the CRL 2-D profiles are flight-level P-3 r_v values.*

3.2 The Example Analysis of Gridded Dual-Doppler TDRs Wind and Reflectivity

To examine the storm and wind structures, the gridded dual-Doppler TDR analysis field of reflectivity and wind at a central time of 2338 UTC on April 13 is shown in Figure 5, which is one of the flight legs sampling a cyclic tornadic supercell storm in Case 10 of VSE18. The chosen height of the gridded dual-Doppler TDR analysis field of reflectivity and wind is located

at 0.75 km AGL (vertical grid spacing is 250 m) to indicate its relative position to the P-3 flight track at the closest height of 0.88 km AGL. The wind field region is smaller than the reflectivity field shown in Figure 5 due to the requirement of dual-doppler wind synthesis, which needs two radar interactions. Reflectivity, on the other hand, does not require two radar interactions in dual-doppler reflectivity synthesis. The dual-Doppler TDR analysis wind field exhibits a counterclockwise spined wind field associated with a mesocyclone at (92.37^{o} W, 32.55^{o} N), which creates positive vorticity leading to vertical upward motion. The cross-section between points A and B (in Figure 5a) shows a convergence area at a distance of 3-5 km from point A at 0.75 km AGL (Figure 5b). The convergent structure associated with a strong updraft is tilted toward to north with height. The core of maximum vertical velocity is at 8-10 km AGL with values greater than 40 m s^{-1}. This strong updraft has the potential to hold more moisture than weak updrafts, potentially leading to a taller cloud top. Moreover, the downdraft is observed at distances of 3 km and 9 km at both 3-4 km AGL in cross-section. The downdraft at the distance of 9 km in the cross-section corresponds to the large radar reflectivity area over 50 dBZ in the northeast of the cross-section (Figure 5a). The 3D map of radar reflectivity shows the title vertical structure at heights of 0.75 km, 5 km, 9 km, and 13 km (Figure 5c).

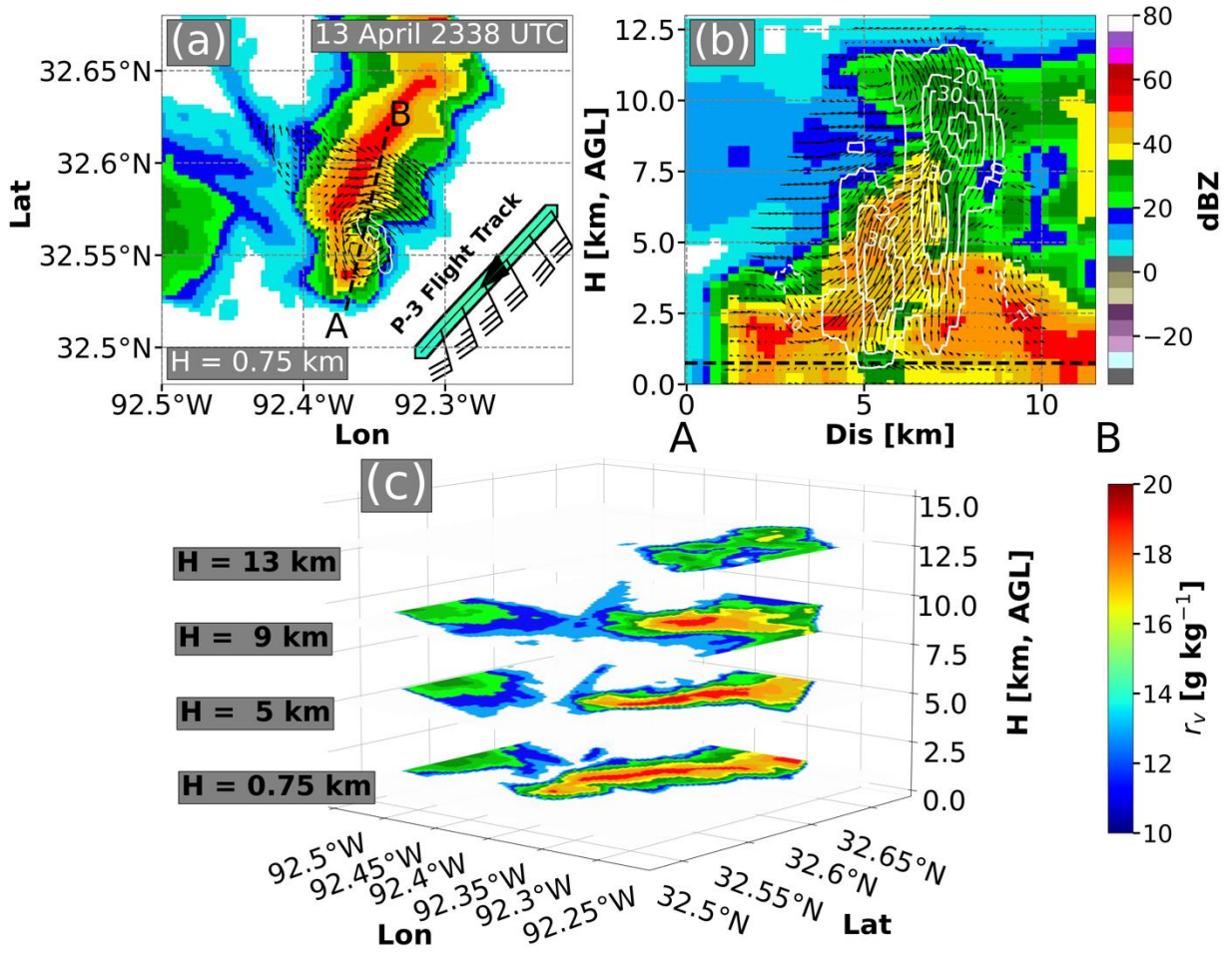

Figure 5. *(a) An example of the gridded dual-Doppler TDR analysis field of reflectivity and wind at 0.75 km AGL at a central time of 2338 UTC on April 13, 2018 – the case 10 in VSE18; The color map indicates radar reflectivity. The color-coded track is the flight-level in situ r_v values. The wind barbs indicate storm-relative flight-level horizontal winds (full barb equals 10 kt; 1 kt ≈0.51 m s^{-1}). The black arrow in the middle of the flight rack indicates the flight direction. (b) A cross-section of the gridded dual-Doppler TDR analysis field of reflectivity and wind between A and B points in panel a. The horizontal black dashed line represents the height of 0.75 AGL of panel a. The solid white contours represent positive vertical velocity, and the dashed white contours represent negative vertical velocity. (c) a 3D radar map showing radar reflectivity at heights of 0.75 km, 5 km, 9 km, and 13 km.*

4. Data Format

The new dataset combining the CRL and TDR measurements from NOAA P-3 aircraft includes convective storm radar reflectivity, 3D winds, CRL sampled convective storm inflow thermodynamic 2D structure, and coordinate information of all cases in VSE18 listed in Table 1. The CRL data for each mission day is saved into a NetCDF file containing related information for each variable. Other than CRL data, aircraft flight location and altitude are provided to geolocate CRL measurements. The images are also provided for each NetCDF file. Near-surface water vapor and temperature data may be contaminated by the surface return due to uncertainties in detecting surface height. Please keep these in mind when you explore CRL data. The TDR data has been formatted in the NetCDF Climate and Forecast (CF) Metadata Conventions format, allowing users to easily process data in three spatial dimensions using the Visualization and Analysis Platform for Ocean, Atmosphere, and Solar Researchers (VAPOR) software developed by the National Center for Atmospheric Research (NCAR) (Li et al. 2019). In order to demonstrate the potential use of the dataset, we utilize VAPOR and present the storm in Figure 5 as the 3D storm structure and its streamlined structures in Figure 6. VAPOR also offers the ability to easily explore other potential plots, such as 2D cross-sections, wind barbs, and contours for the dataset. If you need specific processing of CRL measurements for selected VSE18, please contact the instrument PI (Zhien Wang).

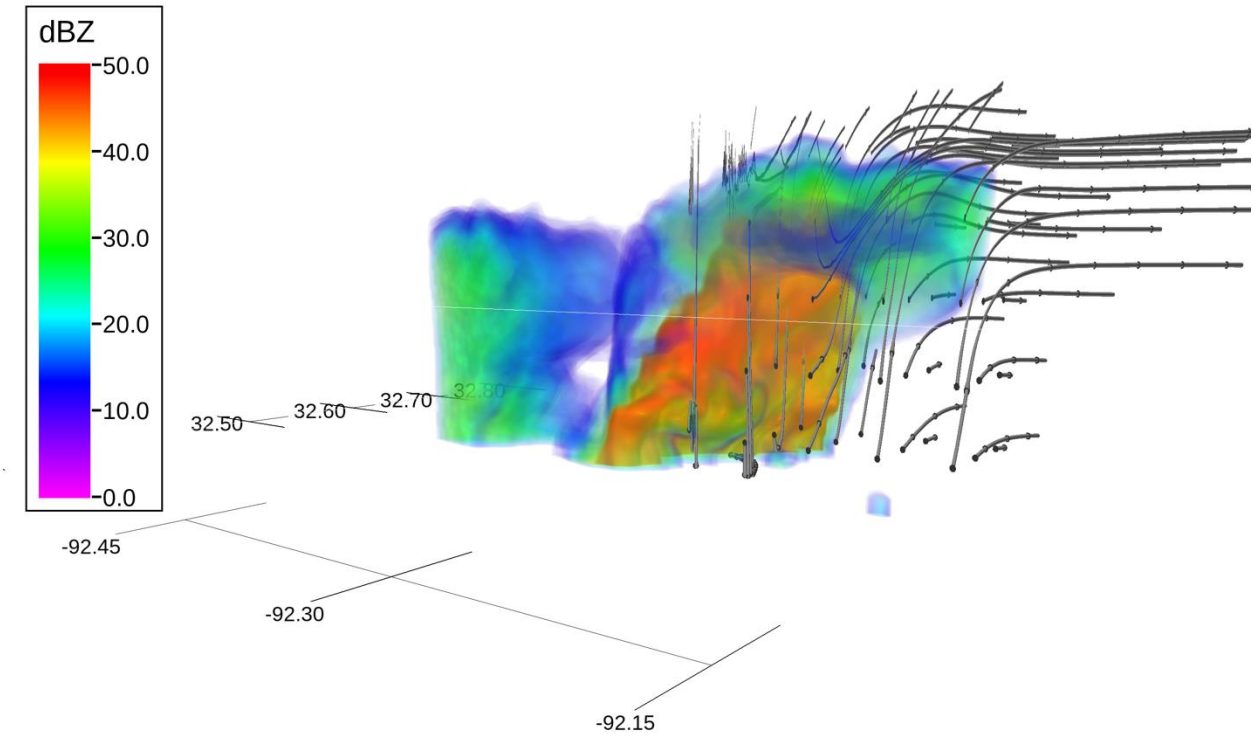

Figure 6*. An example of VAPOR plotted a 3D radar map showing radar reflectivity and streamlines at a central time of 2338 UTC on April 13, 2018, which is the same storm in Figure 5. The color map indicates radar reflectivity. The gray-colored track is the streamline.*

5. Reference

Bergmaier, P. T., B. Geerts, Z. E. Wang, B. Liu, and P. C. Campbell, 2014: A Dryline in Southeast Wyoming. Part II: Airborne In Situ and Raman Lidar Observations. *Monthly Weather Review*, **142,** 2961-2977, https://doi.org/10.1175/Mwr-D-13-00314.1.

Bluestein, H. B., W. P. Unruh, D. C. Dowell, T. A. Hutchinson, T. M. Crawford, A. C. Wood, and H. Stein, 1997: Doppler Radar Analysis of the Northfield, Texas, Tornado of 25 May 1994. *Monthly Weather Review*, **125,** 212-230, https://doi.org/10.1175/1520-0493(1997)125<0212:draotn>2.0.co;2.

Cooney, J., 1970: Remote Measurements of Atmospheric Water Vapor Profiles Using the Raman Component of Laser Backscatter. *Journal of Applied Meteorology*, **9,** 182-184, https://doi.org/10.1175/1520-0450(1970)009<0182:rmoawv>2.0.co;2.

Grasmick, C., B. Geerts, D. D. Turner, Z. Wang, and T. M. Weckwerth, 2018: The Relation between Nocturnal MCS Evolution and Its Outflow Boundaries in the Stable Boundary Layer: An Observational Study of the 15 July 2015 MCS in PECAN. *Monthly Weather Review*, **146,** 3203-3226, https://doi.org/10.1175/mwr-d-18-0169.1.

Jorgensen, D. P., C. L. Ziegler, E. N. Rasmussen, A. S. Goldstein, and A. A. Alford, 2017: Improvements to the NOAA P-3 airborne Doppler tail-mounted radar: Supercell observations from VORTEX-Southeast. *38th AMS Conference on Radar Meteorology, Chicago, IL,Amer. Meteor. Soc.*, **6A.2**, https://doi.org/https://ams.confex.com/ams/38RADAR/webprogram/Paper320666.html.

Li, S., S. Jaroszynski, S. Pearse, L. Orf, and J. Clyne, 2019: VAPOR: A Visualization Package Tailored to Analyze Simulation Data in Earth System Science. *Atmosphere,* **10**, https://doi.org/10.3390/atmos10090488.

Lin, G., C. Grasmick, B. Geerts, Z. E. Wang, and M. Deng, 2021: Convection Initiation and Bore Formation Following the Collision of Mesoscale Boundaries over a Developing Stable Boundary Layer: A Case Study from PECAN. *Monthly Weather Review*, **149,** 2351-2367, https://doi.org/10.1175/Mwr-D-20-0282.1.

Lin, G., B. Geerts, Z. E. Wang, C. Grasmick, X. Q. Jing, and J. Yang, 2019: Interactions between a Nocturnal MCS and the Stable Boundary Layer as Observed by an Airborne Compact Raman Lidar during PECAN. *Monthly Weather Review*, **147,** 3169-3189, https://doi.org/10.1175/Mwr-D-18-0388.1.

Lin, G., Z. Wang, C. Ziegler, X.-M. Hu, M. Xue, B. Geerts, and Y. Chu, 2023: A Comparison of Convective Storm Inflow Moisture Variability between the Great Plains and the Southeastern United States Using Multiplatform Field Campaign Observations. *Journal of Atmospheric and Oceanic Technology*, **40,** 539-556, https://doi.org/10.1175/jtech-d-22-0037.1.

Liu, B., Z. Wang, Y. Cai, P. Wechsler, W. Kuestner, M. Burkhart, and W. Welch, 2014: Compact airborne Raman lidar for profiling aerosol, water vapor and clouds. *Opt Express*, **22,** 20613-20621, https://doi.org/10.1364/OE.22.020613.

Mueller, D., B. Geerts, Z. Wang, M. Deng, and C. Grasmick, 2017: Evolution and Vertical Structure of an Undular Bore Observed on 20 June 2015 during PECAN. *Monthly Weather Review*, **145,** 3775-3794, https://doi.org/10.1175/Mwr-D-16-0305.1.

Philbrick, C. R., 1994: Raman Lidar Measurements of Atmospheric Properties. *P Soc Photo-Opt Ins*, **2222,** 922-931, https://doi.org/Doi 10.1117/12.177985.

Rasmussen, E., 2015: VORTEX-Southeast Program Overview. *National Severe Storms Laboratory Rep.***,** 36 pp.

Turner, D. D., and D. N. Whiteman, 2006: Remote Raman Spectroscopy. Profiling Water Vapor and Aerosols in the Troposphere Using Raman Lidars. *Raman Lidar (RL) Instrument Handbook.*

Wang, Z., 2020: Airborne Compact Raman Lidar (CRL) Water Vapor and Temperature Profiles. Version 2.0, UCAR/NCAR - Earth Observing Laboratory, https://doi.org/https://doi.org/10.26023/JYNH-KCZE-910F. Accessed 20 Feb 2023.

Whiteman, D. N., S. H. Melfi, and R. A. Ferrare, 1992: Raman lidar system for the measurement of water vapor and aerosols in the Earth's atmosphere. *Appl Opt*, **31,** 3068-3082, https://doi.org/10.1364/AO.31.003068.

Wu, D., and Coauthors, 2016: Airborne compact rotational Raman lidar for temperature measurement. *Opt Express*, **24,** A1210-1223, https://doi.org/10.1364/OE.24.0A1210.

Ziegler, C. L., E. N. Rasmussen, T. R. Shepherd, A. I. Watson, and J. M. Straka, 2001: The evolution of low-level rotation in the 29 May 1994 Newcastle-Graham, Texas, storm complex during VORTEX. *Monthly Weather Review*, **129,** 1339-1368, https://doi.org/Doi 10.1175/1520-0493(2001)129<1339:Teollr>2.0.Co;2.

Ziegler, C. L., and Coauthors, 2018: Kinematics, thermodynamics, and microphysics of the tornadic 13-14 April 2018 Calhoun, La supercell during VORTEX-SE. *29th AMS Conference on Severe Local Storms*, Amer. Meteor. Soc., 8.4.